Orbital Maintenance of a Constellation of CubeSats for Internal Gravity Wave Tomography

As Published: 10.1109/JSTARS.2019.2961084

Publisher: Institute of Electrical and Electronics Engineers (IEEE)

Persistent URL: https://hdl.handle.net/1721.1/135979

Version: Final published version: final published article, as it appeared in a journal, conference proceedings, or other formally published context

Orbital Maintenance of a Constellation of CubeSats for Internal Gravity Wave Tomography

Stephen Leroy, Riley Fitzgerald, Kerri Cahoy, *Member, IEEE*, James Abel, and James Clark

***Abstract*—The advent of radio occultation (RO) instruments aboard CubeSats leads to the possibility of a mission to sound atmospheric internal gravity waves if such satellites are deployed in close-flying constellation. The satellites in the constellation must have slightly perturbed orbital inclinations in order to spread the RO soundings within clusters in two horizontal dimensions, and consequently the satellites will disperse because they will experience different rates of regression of nodes. This dispersion must be countered by propulsive maneuvering in order to maintain the close formation of the constellation. Here, a theoretical approach to the necessary propulsive maneuvering is presented and simulations using comprehensive orbit propagators are performed to analyze four propulsive systems: two cold gas propulsion systems and two electrospray propulsion systems. Cold gas propulsion permits greater separations in inclination between satellites in a constellation by virtue of the greater thrust they can exert on a spacecraft: cold gas propulsion can permit inclination separations of 1 to 10° while electrospray limits separations to less than 0.2°. On the other hand, electrospray propulsion provides much longer mission lifetime by virtue of the greater total thrust it offers: cold gas propulsion expends all of its fuel in maintaining the constellation formation in less than approximately 100 days while electrospray propulsion can maintain formation for greater than 1000 days before expending all of its fuel. Mission lifetime is the most critical consideration for a mission, thus electrospray propulsion is recommended for the constellation-flying of CubeSats, but the accelerations that they offer must be greatly increased to enable spacecraft separations useful for tomography of internal gravity waves. Note that any close-flying constellation involving satellites with slightly perturbed inclinations will experience the same dispersing effect as the constellations described herein and, thus, require the same propulsive maneuvering to maintain formation.**

***Index Terms*—Atmospheric waves, propulsion, remote sensing.**

I. Introduction

INTERNAL gravity waves are oscillations in the atmosphere that result from buoyancy as a restoring force [1], [2]. Their wavelengths and frequencies depend on the mechanism that forces them and range typically from 20 to 1000 km in the horizontal, 100 m to 20 km in the vertical, and 10 min to several hours in periodicity. They are generally omnipresent in the Earth's upper troposphere and stratosphere, and the momentum they transport [3] impacts the evolution of the stratospheric Brewer–Dobson circulation and quasi-biennial oscillation [4]–[6], the dynamics of tropospheric jet streaks [7], and convective overshoot [8], and exerts a strong drag and induces intense turbulent mixing in the mesosphere. They can result in bores in both the troposphere [9] and mesosphere [10], the former being able to induce nocturnal convection in the Plains States of the U.S. Their presence in the mesosphere results in the formation of noctilucent clouds [11]. Despite their ubiquity, they have proven elusive because the smallest spatial scale gravity waves are spectacularly difficult to resolve by remote sensing.

Radio occultation (RO) using the global navigation satellite systems (GNSS) [12], [13] is especially sensitive to small vertical scale internal gravity waves [14], [15] whereas high spectral resolution nadir sounders are not [16], [17]. An individual RO sounding of temperature, however, cannot resolve the horizontal structure of a gravity wave, which is necessary to determine the momentum and energy flux transported by the gravity waves present. If multiple RO soundings are obtained within short horizontal and temporal separations of each other, only then can the horizontal structure of the waves present be resolved and the momentum and energy flux be determined using the dispersion relation for internal gravity waves. This concept for inferring gravity waves' momentum flux by RO has been demonstrated, but only for waves with long horizontal scale and periodicity [18], [19] and only for brief intervals in time.

A well-designed constellation of RO satellites flying within a short distance of each other would collect RO soundings that are nearly coincident but separated only by a distance dictated by the constellation configuration and separated in time by less than the smallest possible period of internal gravity waves in the stratosphere, which is approximately 5 min. If the satellites are tightly packed, then a GNSS transmitter that is occulted by the Earth's limb from the vantage point of one RO satellite will also by occulted by the Earth's limb from the vantage point of all of the other RO satellites at nearly the same time but separated in RO sounding location. If the RO soundings are spread well in the two horizontal dimensions, then the vertical phase of the wave at a fixed height in the atmosphere can be manipulated to yield the horizontal wave-vector $\mathbf{k}$, which, in turn, can be used along with the amplitude of the wave in temperature to yield the momentum

Manuscript received June 10, 2019; revised October 4, 2019; accepted December 9, 2019. Date of current version February 12, 2020. The work of S. Leroy was supported by the National Science Foundation under Grant ATM-1850276 in addition to discretionary funding from Atmospheric and Environmental Research, Inc. The work of R. Fitzgerald was supported by a Draper Laboratory Fellowship. *(Corresponding author: Stephen Leroy.)*

S. Leroy is with the Atmospheric and Environmental Research, Inc., Lexington, MA 02421 USA (e-mail: sleroy-at-aer.com).

R. Fitzgerald, K. Cahoy, and J. Abel are with the Massachusetts Institute of Technology, Cambridge, MA 02139 USA (e-mail: rmfitz@mit.edu; kcahoy@mit.edu; jmabel@mit.edu).

J. Clark is with the Aero/Astro, Massachusetts Institute of Technology, Cambridge, MA 02139 USA (e-mail: jimclark@mit.edu).

Digital Object Identifier 10.1109/JSTARS.2019.2961084

and energy flux transported by the wave. This technique is *internal gravity wave tomography*. Because of the complex geometry of RO and its sampling distribution, configuring a constellation that is well suited to internal gravity wave tomography requires careful trade studies. This work commences such studies. (The design of such a constellation is described verbally in Section II and mathematically in Appendix A.)

GNSS RO is now being performed by 3 U and 6 U CubeSats, enabling future low-cost RO constellations [20]. Orbit control is necessary for countering the effects of orbital precession effects induced by the Earth's equatorial bulge and other naturally occurring forces that tend to disperse constellations of CubeSats. If the satellites are deployed into orbits with different inclination, propulsion becomes necessary to tilt the satellites' orbit planes and counter the effects of differential regression of nodes. Current demonstrated RO CubeSats lack on-board propulsion, however, and planned propulsion on-board RO CubeSats will be constraining: limitations on total ΔV will constrain the amount of time a constellation of RO CubeSats can fly in a close formation, and limitations on the amount of acceleration the propulsion can provide will constrain the separation of the satellites within the constellation. This research is a study of the consequences of limited propulsion on the lifetime of a mission to perform internal gravity wave tomography and how widely spaced the CubeSats within that constellation can be.

The article is organized as follows. The second section illustrates how an RO constellation obtains clusters of RO soundings suited to internal gravity wave tomography assuming Keplerian orbits. The third section describes the complication introduced by orbit tilting and differential regression of nodes. The fourth section assumes a realistic orbit propagator, including a comprehensive gravitational model for the Earth and perturbations by the Sun, Moon, and planets as well as variable neutral atmospheric drag. An equation relating the spatial separation of soundings and characteristics of spacecraft propulsion to the lifetime of a gravity wave tomography mission and its occultation yield is given. The fifth section summarizes the results.

II. RO Tomography of Internal Gravity Waves

A constellation of RO satellites designed for internal gravity wave tomography will yield clusters of RO soundings that are spread in two horizontal dimensions on the Earth, yielding a daily number of clusters equal to the number of RO soundings obtained by any one of the RO satellites, every RO sounding belonging to a cluster. For tomography to work, the clusters of RO soundings must be spread in both horizontal dimensions, thus, the RO satellites must also be spread in two dimensions. Systematic clustering of the RO soundings over the duration of a mission dictates that the RO satellites never spread too far apart. Configuring a constellation of RO satellites that is spread in two dimensions and yet does not disperse is the central challenge.

The constellations will be built on the notion of mutual orbiting groups. In such groups, a number of satellites follow each other in a trajectory about a virtual circular orbiter, which serves as a reference. This is accomplished by matching their mean motions, assigning them a nonzero eccentricity far less than unity ($e \ll 1$) to extend their mutual orbit axis in the orbital velocity direction, and tilting their angular momentum vectors by an angle δ with respect to the reference orbiter to extend their mutual orbit axis in the direction perpendicular to the orbit velocity direction. The length of the axis in the orbit velocity direction is $4ae$ and the length of the perpendicular axis is $2a\delta$, with a the semimajor axis of the mutual orbit; see Fig. 7 in Appendix A, which contains a detailed description of the construction of mutual orbit groups.

TABLE I
Simple Keplerian Constellation

sat	e	i	Ω	ω	ν
1	0.01	51.42°	0.0°	-90.00°	91.15°
2	0.01	51.86°	0.0°	90.00°	-91.15°
3	0.01	51.64°	0.29°	179.82°	172.53°
4	0.01	51.64°	-0.29°	0.18°	-7.77°

All satellites have a semimajor axis $a = R_E + 404$ km.

A simple constellation of four satellites is described by orbital elements in Table I, constituted of two pairs of mutual orbiting RO satellites in orbits with altitude 404 km and inclinations near $i = 52.6°$, characteristic of the International Space Station (ISS). RO geolocations were simulated for an oblate Earth (equatorial radius $R_E = 6378.137$ km, polar radius R_P, and $(R_E - R_P)/R_P = 1/298.3$) with forward and aft-viewed RO events within 60° boresight of the satellite velocity vector. Both the U.S. GPS and the Russian GLONASS transmitters are used in RO, and their orbits are taken from their two-line elements as of March 6, 2018. The orbital elements e, i, Ω, ω, and ν are the eccentricity, inclination, right ascension of the ascending node (RAAN), argument of perigee, and true anomaly at epoch. One day of simulated geolocations for RO soundings for this constellation of satellites yields ∼1400 clusters of soundings that can be used for internal gravity wave tomography.

Fig. 1 shows a map of all RO soundings and five clusters of RO soundings taken from one day of simulated RO geolocations. In gravity wave tomography, the vertical structure of the wave is analyzed in each of the temperature soundings of a cluster of soundings. The phase of the wave at a specified height is determined for each sounding, and those phases can be analyzed to determine the horizontal wave-vector $\mathbf{k}$ of the wave. The amplitude of the wave in temperature, the three-dimensional wave-vector, and the gravity wave dispersion relation suffice to compute the momentum flux transported by the wave. The method has been demonstrated previously [18], [19], but a dedicated mission for gravity wave tomography like this has not yet been conceived or deployed.

III. Constellation Maintenance Strategy

A constellation for internal gravity wave tomography by RO requires maintenance, because natural perturbations to the orbits of the individual satellites cause them to disperse. The most significant orbital perturbation that leads to dispersion is the oblate-Earth J_2 effect, which induces rates of regression of nodes and precession of perigee that are different among the satellites. The rates of regression of nodes $\dot{\Omega}$ and perigee precession $\dot{\omega}$

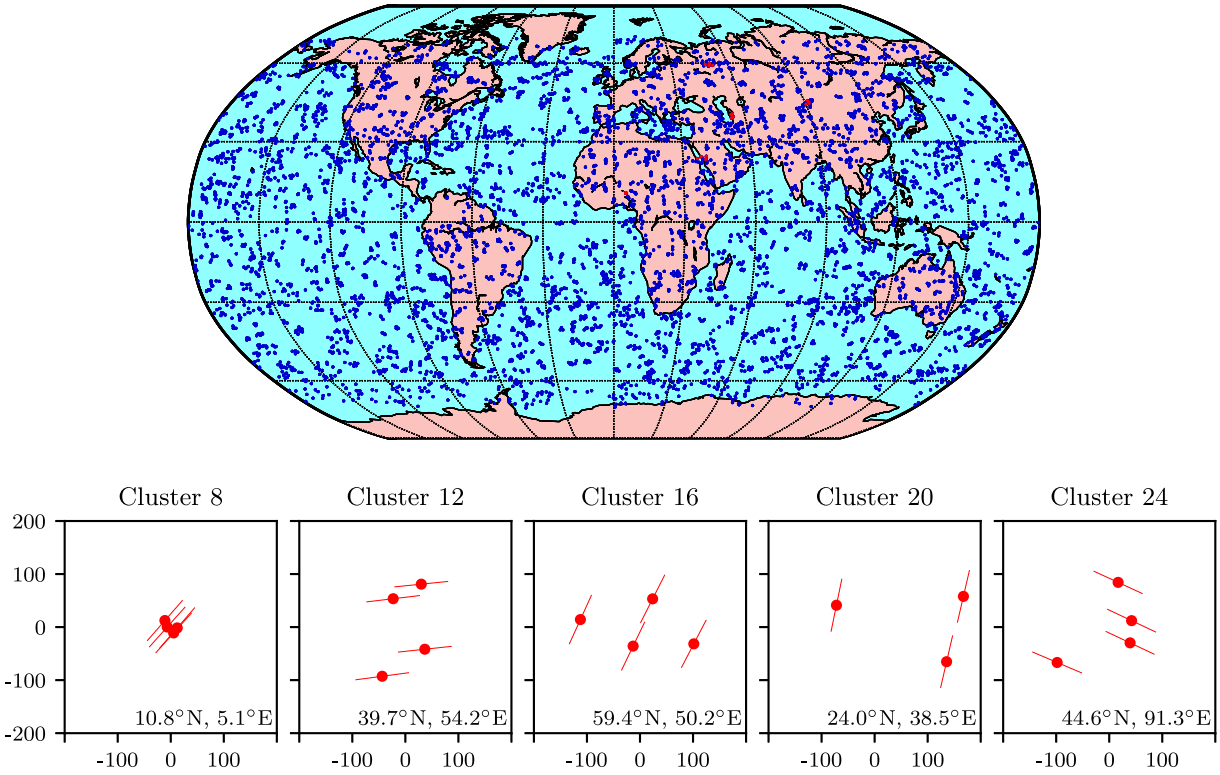

Fig. 1. All RO soundings in a day and five select clusters of soundings. All the RO soundings obtained by the constellation described in Table I are plotted. Rising and setting occultations are retained for GPS and GLONASS navigation systems as of March 6, 2018 within 60° of the fore- and aft-velocity directions. Five clusters arbitrarily selected to illustrate the variety distributions of RO soundings in a cluster are also shown. The x- and y-axes are eastward and northward horizontal positions in units of kilometers. The lines through each point indicate the orientation of the RO ray-path. The latitude and longitude of the center of each cluster is given in the lower right corner of each plot.

for a satellite with inclination i, mean motion n, and semilatus rectum p are

$$\dot{\Omega} = -\frac{3}{2} n J_2 \left(\frac{R_E}{p}\right)^2 \cos i \tag{1a}$$

$$\dot{\omega} = \frac{3}{2} n J_2 \left(\frac{R_E}{p}\right)^2 \left(2 - \frac{5}{2}\sin^2 i\right). \tag{1b}$$

If the satellites in the constellation have different inclinations, their precession rates will differ and the co-orbiting constellation will disperse rapidly even if the satellites' periods are matched. Fig. 2 illustrates the effect of the differential precession in both Ω and ω.

In order to keep the satellites of the constellation from dispersing, the precession rates of the orbital planes and the rates of change of the mean true longitude $\dot{\bar{l}}$ must be matched. Matching their mean motions $\dot{\bar{l}}$ is relevant because satellites in orbits with the same semimajor axis but slightly different inclinations experience not only different rates of regression of nodes but also different rates of precession of perigee, and the latter will cause the satellites to revolve around the Earth's spin axis at different rates over long periods of time. Explicitly, the matching conditions are

$$\Delta\dot{\Omega} = 0 \tag{2a}$$

$$\Delta\dot{\bar{l}} = \Delta n + \Delta\dot{\omega} + \Delta\dot{\Omega} = 0 \tag{2b}$$

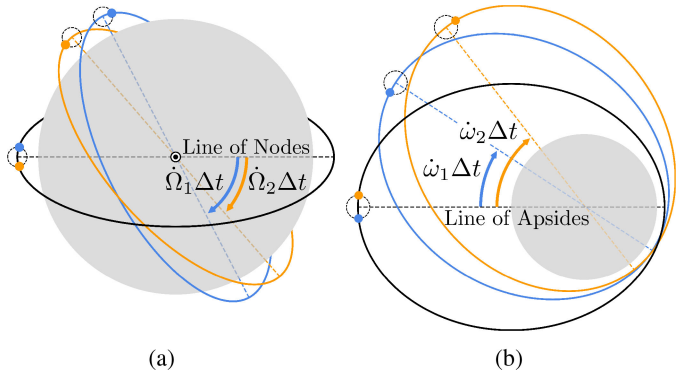

Fig. 2. Differential precession rates cause the co-orbiting arrangement to separate over time. (a) RAAN. (b) Argument of Perigee.

where $\bar{l} = M + \omega + \Omega$ is the mean true longitude and the Δ's denote a difference between the element for a specific satellite and that of a reference orbit. Both of these conditions must be satisfied, and the only two ways to do so are by orbit design and by propulsive maneuvering. Since the orbits' inclinations and eccentricities are used to prescribe the constellation formation, the only orbital parameter that can be used to tune $\Delta\dot{\Omega}$ and $\Delta\dot{\bar{l}}$ is the semimajor axis a (and thus also p). The changes in the rates of regression of nodes and precession of perigee and change in mean motion when a satellite is subjected to a change

in a are

$$\frac{\partial \dot{\Omega}}{\partial a} = -\frac{7}{2}\frac{\dot{\Omega}}{a} \tag{3a}$$

$$\frac{\partial \dot{\omega}}{\partial a} = -\frac{7}{2}\frac{\dot{\omega}}{a} \tag{3b}$$

$$\frac{\partial n}{\partial a} = -\frac{3}{2}\frac{n}{a} \tag{3c}$$

where $\dot{\Omega}$ and $\dot{\omega}$ are the precession rates of the reference orbiter. If a is considered the same for all satellites in the constellation, then satellite j would have matching n but nonzero differential precession rates $\Delta\dot{\Omega}_j$ and $\Delta\dot{\bar{l}}_j$, thus violating the conditions of (2). For satellite j, the amount by which the semimajor axis would have to be adjusted to bring either $\dot{\Omega}$ or $\dot{\bar{l}}$ into agreement with the reference orbiter would be

$$\Delta a_{\dot{\Omega}} = \frac{2a}{7}\frac{\Delta\dot{\Omega}_j}{\dot{\Omega}} \tag{4a}$$

$$\Delta a_{\dot{\bar{l}}} = 2a\frac{\Delta\dot{\omega}_j + \Delta\dot{\Omega}_j}{3n + 7\dot{\omega} + 7\dot{\Omega}} \approx \frac{2a}{3}\frac{\Delta\dot{\omega}_j + \Delta\dot{\Omega}_j}{n} \tag{4b}$$

in which $n \gg \dot{\omega}, \dot{\Omega}$ is assumed: precession rates are typically three orders of magnitude less than a low-Earth-orbiting satellite's mean motion because $J_2 = 1.08263 \times 10^{-3}$ for the Earth. Since $n \gg \dot{\Omega}$, dispersion in mean true longitude can be prevented by adjusting a by an amount much less than what is required to prevent dispersion in ascending node, and doing so would require propulsion to prevent dispersion in ascending node. If instead dispersion in ascending node were to be prevented by adjusting a, then no amount of propulsion could prevent dispersion in mean true longitude. The design and deployment of the constellation must: 1) correct for in-plane differential rates by semimajor axis adjustments according to (4b), and 2) correct for differential plane precession rates using propulsion.

The non-Keplerian orbital perturbations incurred by J_2 forcing lead to demands on propulsion in order to maintain a constellation intended for internal gravity wave tomography. While other naturally occurring forces, such as neutral atmospheric drag, can lead to dispersion of the constellation, their differential as experienced by the satellites in the constellation are expected to be substantially less than those that lead to differential regression of nodes. Deployment of the constellation will require propulsive maneuvering in order to tilt the orbit planes into slightly different inclinations and to tune the semimajor axes to match the motions of the mean true longitude for the satellites in the constellation. After deployment, propulsion is needed throughout the lifetime of the mission to prevent dispersion in an ascending node.

The two sections that follow contain: 1) a theory for the rate of propulsion expenditure; and 2) simulations that show likely rates of propulsion expenditure. Two parameters of the propulsion will ultimately dictate the lifetime of a mission involving a constellation of CubeSats, such as one intended for tomography of internal gravity waves, that requires relative station keeping.

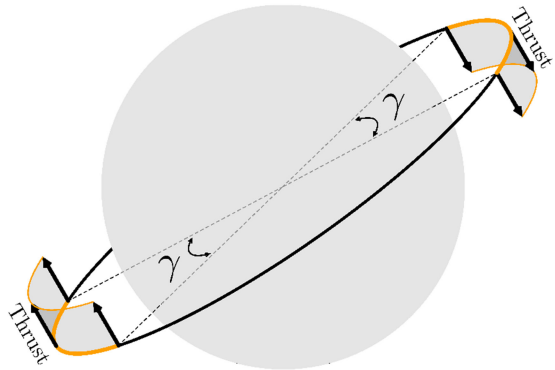

Fig. 3. Geometry of propulsive maneuvers to counter-act the differential regression of nodes. The burns occupy orbit arcs of γ radians centered about maximum and minimum latitude; i.e., where the argument of latitude ℓ is $+90^\circ$ and -90°, respectively. Impulses directed toward the equator plane acts to increase the RAAN for a prograde orbit.

IV. Rate of Propulsion Expenditure: Theory

The theoretical rate of propulsion expenditure necessary to keep an individual satellite near the reference orbiter is limited by the finiteness of propulsion per unit mass of the spacecraft it can exert. A theoretical derivation of the rate of propulsion expenditure begins with the assumption of infinite propulsion per unit mass available, which makes the impulsive maneuvers perfectly efficient, and ends with a relaxation of that assumption, allowing for inefficiency in the impulsive maneuvers.

The maneuvers required to counteract the differential regression of nodes must augment or diminish the perturbations of J_2, which are greatest when the subspacecraft point is at an extremum in latitude; i.e., where the *argument of latitude* $\ell = \omega + \nu = \pm 90^\circ$ (with ν the true anomaly of the satellite). The amount of impulse needed by a satellite in the constellation at $\ell = \pm 90^\circ$ is determined by the amount of differential regression of nodes $\Delta\dot{\Omega}_j$ that the impulse must counteract. The specific time-averaged torque needed to counteract differential regression of nodes is given by

$$\boldsymbol{\tau} = -\Delta\dot{\Omega}_j\, \hat{\mathbf{z}} \times \mathbf{l}_j \tag{5}$$

with $\mathbf{l}_j$ the angular momentum of the satellite j in the constellation and $\hat{\mathbf{z}}$ a unit vector pointing in the direction of the Earth's spin axis. Propulsive maneuvers must be conducted as illustrated in Fig. 3, with γ the length of orbit arc (in radians) about $\ell = \pm 90^\circ$ over which propulsion is applied. When propulsion is applied, it is oriented parallel or antiparallel to the orbit's mean angular momentum vector. On the RO CubeSat, the propulsion is exerted perpendicular to the direction of the CubeSat's motion and to the zenith direction. If propulsive maneuvers are exerted every N orbits, then the time mean torque applied by the propulsive maneuvers must match the torque required of (5)

$$\frac{1}{2\pi N}\int_0^{2\pi/n_j} \mathbf{r} \times \frac{\mathbf{T}}{m}\, n_j\, dt = \boldsymbol{\tau} \tag{6}$$

in which $\mathbf{T}$ is the force being applied to the satellite with mass m and $\mathbf{r}$ is the position of the satellite with respect to the Earth's center of mass. In the limit of very small orbital eccentricity

($e \ll 1$) with $|\mathbf{l}| = \sqrt{\mu a_j}$, (5) and (6) can be evaluated to yield

$$\sqrt{\frac{\mu}{a_j}} \sin i_j \, |\Delta\dot{\Omega}_j| = \frac{\gamma \alpha_{\max}}{N\pi} \operatorname{sinc} \gamma/2. \tag{7}$$

The left-hand side of the equation should be interpreted as a property of the orbit of satellite j that can be evaluated as a function of only its Keplerian orbital elements. The right-hand side describes the requirements on the propulsive maneuvers needed to keep the satellite within the formation of the constellation.

Maximum efficiency of propulsion expenditure is attained when the impulsive maneuvers take place at precisely $\ell = \pm 90^\circ$, meaning the orbit arc of propulsion expenditure $\gamma = 0$ and the maximum propulsion available to the satellite $\alpha_{\max} = |\mathbf{T}|/m$ is infinite (with m the mass of the spacecraft). In this case, the ideal time-average expenditure of propulsion ΔV, $\bar{\alpha}^*$, is given by

$$\bar{\alpha}_j^* = \frac{1}{N\pi} \lim_{\gamma \to 0} \gamma \alpha_{\max} = \sqrt{\frac{\mu}{a_j}} \sin i_j \, |\Delta\dot{\Omega}_j|. \tag{8}$$

This is the minimum rate with which ΔV can be expended to maintain relative station keeping for satellite j of the constellation. "Propulsion" and "ΔV" are used interchangeably, because the amount of velocity change ΔV that the fuel on board a satellite can impel the satellite serves as a useful measure of the total amount of propulsion on board.

The maximum propulsive acceleration $\alpha_{\max}$ available is finite, however, and, consequently, a realistic scenario for propulsive maneuvers must have them take place over finite nonzero orbit arcs $\gamma > 0$. The orbit is said to be efficient with efficiency η that relates the actual rate of propulsion expenditure to the ideal rate of propulsion expenditure

$$\bar{\alpha}_j \equiv \bar{\alpha}_j^*/\eta. \tag{9}$$

Combining (7), (8), and (9) and considering that the actual rate of ΔV consumption $\bar{\alpha}_j$ is related to the maximum available propulsive acceleration through $\gamma \alpha_{\max} = N\pi\bar{\alpha}_j$ results in an equation for the efficiency η

$$\eta = \operatorname{sinc} \gamma/2. \tag{10}$$

The term $\bar{\alpha}_j^*$ is best interpreted as a property of the satellite's orbit resulting from a requirement on torque to counter the differential regression of nodes and $\alpha_{\max}$ as a property of the spacecraft resulting from its propulsive capability and mass. Noting that (10) can be rewritten as $\gamma = 2\sin^{-1}(\gamma\eta/2)$, the actual rate of propulsion expenditure $\bar{\alpha}_j$ is related to the spacecraft propulsive capability $\alpha_{\max}$ through

$$\bar{\alpha}_j = \frac{2\alpha_{\max}}{N\pi} \sin^{-1}\left(\frac{N\pi}{2} \frac{\bar{\alpha}_j^*}{\alpha_{\max}}\right). \tag{11}$$

This equation gives the theoretical rate of propulsion expenditure for a satellite with finite on-board propulsion capability that must counter the differential rate of regression of nodes among the satellites in the constellation: $\bar{\alpha}_j^*$ is a property of the orbit specified for satellite j (i.e., its Keplerian orbital elements), $\alpha_{\max}$ the propulsive capability of the spacecraft, and N a designation for how many orbits should elapse between propulsive maneuvers.

A satellite remains a part of the constellation as long as it retains propulsion on board to be used to counter the differential regression of nodes. When it completely expends its on-board propulsion, the differential regression of nodes can no longer be countered, and the satellite will drift away from the reference orbiter and consequently the rest of the constellation. A constellation's lifetime is governed by the amount of time elapsed before any one of the satellites in the constellation drifts out of the formation, which always occurs for the satellite with the largest inclination separation Δi from the reference orbiter (assuming no spacecraft malfunction). The largest value of Δi in a constellation is $\max(\Delta i) = \delta$.

Fig. 4 shows the relationship between the theoretical rate of propulsion expenditure $\bar{\alpha}_j$ and the maximum acceleration $\alpha_{\max}$ provided by the on-board propulsion system for different numbers of orbits between propulsive maneuvers N. The theoretical rate of ΔV expenditure $\bar{\alpha}_j$ is best interpreted as the inverse of the length of time that satellite j remains in the constellation. Two conclusions can be drawn from Fig. 4 and (11). First, the efficiency of propulsive maneuvering $\eta = \bar{\alpha}_j^*/\bar{\alpha}_j$ increases with greater propulsive capability $\alpha_{\max}$. For each value of N, all curves approach the same value of $\bar{\alpha}_j$ as $\alpha_{\max} \to \infty$, and that value is the ideal rate of propulsion expenditure $\bar{\alpha}_j^*$. Second, the longer one waits between propulsive maneuvers (i.e., the greater the value of N), the greater the rate of propulsion expenditure and the shorter the mission lifetime ($\bar{\alpha}_j^{-1}$) for a specific propulsive capability $\alpha_{\max}$.

V. Rate of Propulsion Expenditure: Simulations

In practice, the rate of propulsion expenditure depends on many influences in addition to the orbital perturbations induced by J_2, such as higher order terms in the Earth's gravity field, gravitation by other celestial bodies, and neutral atmosphere drag. Consequently, the spacecraft must be subjected to propulsive maneuvers *conditionally* rather than *prognostically*. The propulsion will occur at irregular intervals, and the propulsion expenditure curves will deviate from the theoretical curves of Fig. 4. In this section, a simple pair of rules is prescribed to keep an individual satellite in a desired position relative to the reference orbit. Two sets of simulations are, then, performed: the first to investigate the theoretical rates of propulsion expenditure when relative station-keeping rules are implemented, and the second to illustrate the trade space of satellite spacing and mission lifetime for four existing propulsion systems.

A simple pair of rules to keep an individual satellite in a desired position relative to the reference orbit is given as these *relative station-keeping rules.*

1) An upper bound is placed on the RAANs such that $|\Omega_j - \Omega_{\text{ref}}| < \Delta\Omega_{\max}$ for satellite j in the constellation.
2) When the above rule is violated for any satellite, execute a pair of propulsive maneuvers of ΔV_{cor} at maximum and minimum subspacecraft latitude $\ell = \pm 90^\circ$.

The maximum allowable departure $\Delta\Omega_{\max}$ of the RAAN for a given satellite from that of the reference orbiter and the size of the impulse ΔV_{cor} are free, tunable parameters. The

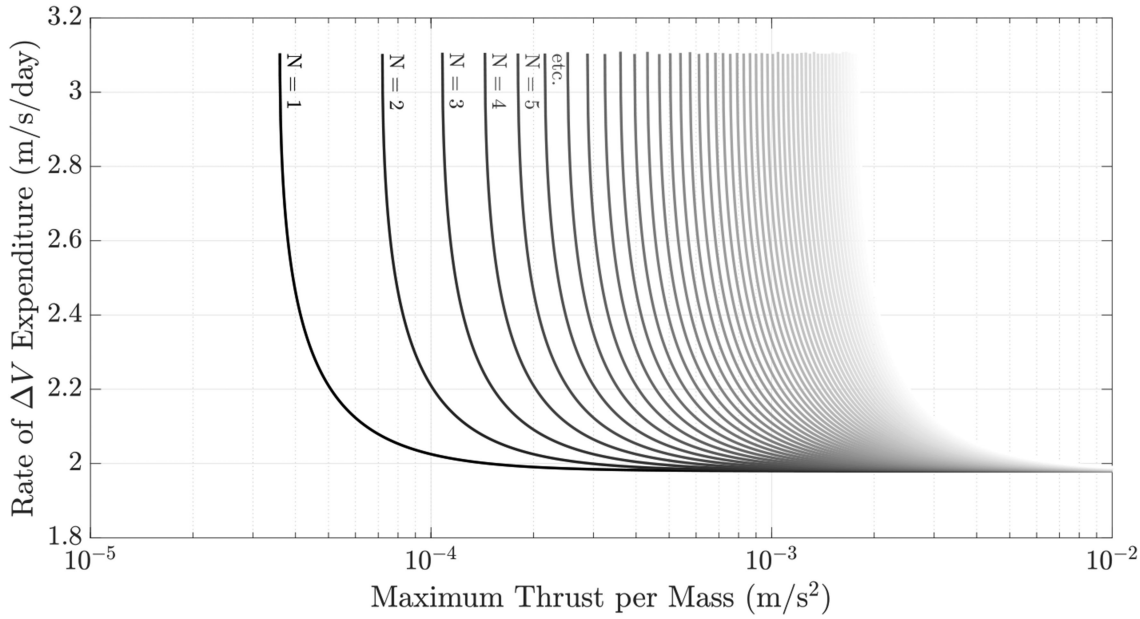

Fig. 4. Rate of propulsion (ΔV) expenditure, $\bar{\alpha}_j$, as a function of the propulsion per mass available to the spacecraft $\alpha_{\max}$ for varying numbers N of orbits between propulsive maneuvers. For a constellation in an orbit characteristic of the ISS (altitude 400 km, inclination 51.4°) and CubeSat separation angle $\delta = \Delta i = 0.172^\circ$, the ideal (minimum) rate of propulsion expenditure is $\bar{\alpha}^* = 1.98$ m s^{-1} day^{-1}. An RO CubeSat of 6 U form factor can exert up to $\approx$3000 m s^{-1} of total ΔV if electrospray propulsion is implemented or $\approx$60 m s^{-1} if cold gas propulsion is implemented.

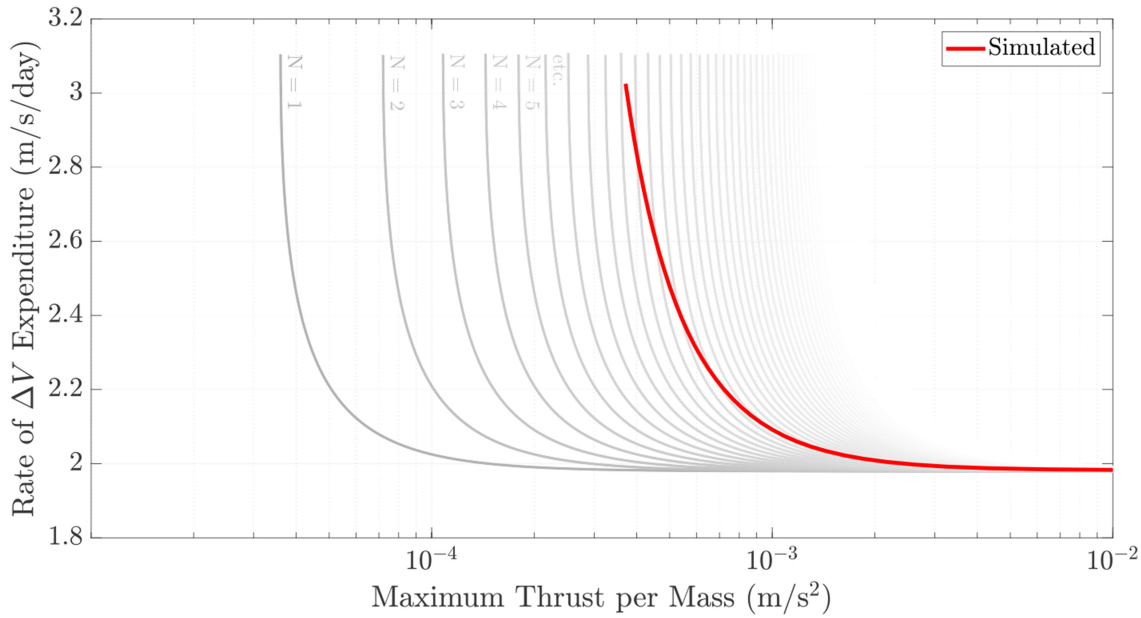

Fig. 5. Rate of propulsion (ΔV) expenditure for a mission defined by a simple condition and rule: $|\Omega_j - \Omega_{\text{ref}}| < 0.01^\circ$ and 1 m s^{-1} burns at maximum and minimum latitudes. The red curve is the result of 36 simulations. Gray curves are the theoretical curves derived in Section IV and taken from Fig. 4.

parameter $\Delta\Omega_{\max}$ is referred to as the *RAAN departure tolerance* hereafter.

The results for the first set of simulations are shown in Fig. 5. It shows a curve of rate of propulsion expenditure $\tilde{\alpha}$ for an orbit conditioned on the rules of relative station-keeping defined above. The RAAN departure tolerance is set to $\Delta\Omega_{\max} = 0.01^\circ$ and the impulses set to $\Delta V_{\text{cor}} = 1$ m s^{-1}. The orbit propagator consists only of the Earth's gravitational central force and the J_2 quadrupole perturbation. The relative station-keeping rules are implemented through Astrogator of the Systems Tool Kit (STK). Each mission is simulated until the total propulsion expended is 1000 m s^{-1}. The effective burn arc γ is calculated, and the actual rate of propulsion expenditure $\tilde{\alpha}$ is computed at the end of each simulation. The theoretical curves of (11) are valid but the

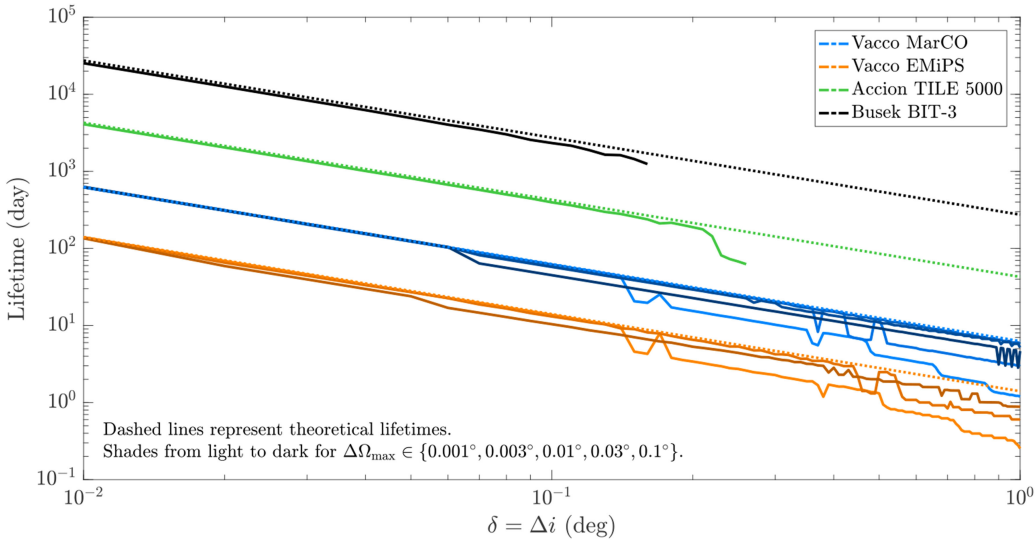

Fig. 6. Constellation lifetime versus the separation δ for varying amounts of RAAN tolerance $\Delta\Omega_{\max}$ and for four different propulsion systems. The simulations are described in the text. Theoretical lifetime (dashed line) and lifetime from orbit simulations (solid curves) are shown for four different propulsion systems as indicated by the legend in the upper right corner of the plot. Five different values for $\Delta\Omega_{\max}$ ($0.001°$, $0.003°$, $0.01°$, $0.03°$, and $0.1°$) are simulated for the Vacco MarCO and EMiPS propulsion systems with lighter colors for the smaller values of RAAN tolerance.

value of N changes based on spacecraft propulsive capability. The approximate rate of propulsion expenditure is

$$\tilde{\alpha}_j \simeq \alpha_j^* \Big/ \operatorname{sinc}\left(\frac{n\Delta V_{\text{cor}}}{2\alpha_{\max}}\right) \tag{12}$$

derived under the approximation that impulses are exerted at semiregular intervals. The relative station-keeping rules lead to a long-term average value for N of

$$\tilde{N} = \frac{2\alpha_{\max}}{\pi\bar{\alpha}^*} \sin\left(\frac{n\Delta V_{\text{cor}}}{2\alpha_{\max}}\right) = \frac{n}{\pi}\frac{\Delta V_{\text{cor}}}{\tilde{\alpha}} \tag{13}$$

which can be seen to vary with $\alpha_{\max}$ as shown in Fig. 5. Smaller spacecraft propulsive acceleration $\alpha_{\max}$ requires longer impulse arcs to achieve the same impulse, and thus the impulse is made less efficient and more frequent impulses become necessary—smaller N—to counter the effects of differential regression of nodes.

The RAAN departure tolerance $\Delta\Omega_{\max}$ and ΔV_{cor} are not wholly independent; in fact, they can be chosen to optimize the rate of propulsion expenditure $\tilde{\alpha}$. The rate of propulsion expenditure is minimized if the impulse ΔV_{cor} is chosen such that each burn yields an absolute change of the RAAN of $|\Delta\Omega_{\max}|$. After two burns, at $\ell = -90°$ and $\ell = +90°$, the absolute change in RAAN should be $2|\Delta\Omega_{\max}|$, taking the satellite either from $\Delta\Omega = -|\Delta\Omega_{\max}|$ to $\Delta\Omega = +|\Delta\Omega_{\max}|$ or vice versa. This optimal selection for ΔV_{cor} is

$$\Delta V_{\text{cor}} = \frac{2\alpha_{\max}}{n} \sin^{-1}\left|\frac{n^2 a \sin i}{2\alpha_{\max}} \Delta\Omega_{\max}\right|. \tag{14}$$

The required correction impulse is generally insensitive to maximum available propulsive acceleration $\alpha_{\max}$ for large values of $\alpha_{\max}$, but when maximum available propulsive acceleration is comparable to or less than $n^2 a$, the required correction impulse increases greatly.

TABLE II
PROPULSION SYSTEMS

System	$\alpha_{\max}$ (m s^{-2})	ΔV_{total} (m s^{-1})
Vacco MarCO	693.42	60.75
Vacco EMiPS	82.29	15.68
Accion TILE 5000	11.68	450.21
Busek BIT-3	9.09	2965.40

The results for the second set of simulations are shown in Fig. 6. In the simulations, each spacecraft has a mass of 10 kg, which approximates a 6 U CubeSat. The separation δ of the satellites within the constellation is varied from $0.01°$ to $1°$ in order to show the relationship between separation and mission lifetime. Four representative CubeSat propulsion systems are assessed: the Vacco JPL Micro Propulsion System (MarCO), the Vacco End-Mounted Standard Micro-Propulsion System (EMiPS), the Accion TILE 5000, and the Busek BIT-3. The first two are cold gas propulsion systems, and the last two are electrospray systems. Their maximum accelerations (thrust per unit mass) and total ΔV are summarized in Table II. In general, cold gas propulsion systems are characterized by much greater available thrust and much less total thrust than electrospray systems, as is clear in the parameters given in Table II. The comprehensive orbit simulator of NASA's General Mission Analysis Tool (GMAT) is used for orbit propagation. GMAT is used here instead of STK (as was used for Fig. 5) because it is better suited to scripting a large ensemble of runs. In order to demonstrate that the relative station keeping rules suffice to maintain the constellation formation, neutral atmospheric drag and a complete gravitational environment are included in the propagator. Consistent with Figs. 4 and 5, the orbits are characteristic of that of the ISS. Only the orbits of the satellites with $\Delta i = \delta$ are simulated as for Fig. 5, corresponding to the satellites with the largest dispersion rates $\dot{\Omega}$ with respect to the reference orbiter. That the satellites remained in close-flying formation

was checked quantitatively for a few of the simulations. No accounting is made for the propulsion required for the initial configuration of the constellation.

Fig. 6 reveals the central tradeoff between cold gas propulsion and electrospray propulsion for CubeSats: cold gas propulsion permits great separations δ between the satellites in a constellation, and electrospray propulsion permits much longer mission lifetimes. The fundamental limit on the separation δ of the satellites in the constellation is that only so much propulsion can be spent in a half orbit ($\gamma = \pi$) to counter the effects of the differential regression of nodes. Systems with lower available propulsive acceleration $\alpha_{\max}$ can do less to counter the differential regression of nodes. Since larger separations δ lead to higher rates of dispersion, less available acceleration means a lower limit on the separation δ. The satellites configured with the electrospray Accion Tile 5000 and the Busek BIT-3 propulsion systems can only maintain formation for separations less than 0.26° and 0.16°, respectively. The satellites configured with cold gas Vacco MarCO and Vacco EMiPS propulsion systems can maintain formation for separations δ of 12° and 1.4°. On the other hand, the larger total values of ΔV available with electrospray propulsion systems means that those constellations can maintain formation for much longer, thus meaning longer mission lifetimes for a given separation δ than cold gas propulsion systems can. For a separation $\delta = 0.1^\circ$, the Busek BIT-3 and the Accion TILE 5000 electrospray propulsion systems can keep a constellation in formation for 2300 and 240 days while the Vacco MarCO and EMiPS cold gas propulsion systems keep the formation intact for only approximately 80 and 20 days, respectively. Mission lifetime is inversely proportional to the separation δ for any given propulsion system.

VI. Summary

An exposition of the lifetime of a mission involving CubeSats flying in a tight formation is presented above. While the findings of this research are directly applicable to any constellation of CubeSats that requires close formation flying with small departures in orbital inclination i, the particular focus is a mission intended to sound internal gravity waves in the atmosphere. The formation is one in which the satellites appear to orbit around a reference satellite in a circular orbit about the Earth, the extent of the "mutual" orbit in the orbital velocity direction being given by $4ae$ and the extent in the transverse orbital velocity direction by $2a\delta$, with a the semimajor axis of the reference orbiter and e and δ the eccentricity of the mutual orbiter and the angle separating the angular momentum vectors of the reference and mutual orbiters. A constellation formed this way experiences dispersion due to natural forces, primarily that of the J_2 term of the Earth's gravitational field. Because the satellites' orbits have slightly different inclinations, each satellite experiences a different rate of regression of nodes. Maintaining the formation requires propulsion to counter the differential rates of regression of nodes, with impulses directed either parallel or antiparallel to the orbit's angular momentum vector when the spacecraft is at or near argument of latitude $\ell = \pm 90^\circ$. Limitations on the amount of acceleration provided by the on-board propulsion decreases the efficiency of the available propulsion and severely restricts the maximum separation of the satellites δ in the constellation. Also, the limited amount of on-board propulsion ultimately dictates the lifetime of the mission: after a satellite's propulsion is entirely consumed, it will drift out of the formation in a matter of weeks.

The equation describing the lifetime of the mission is a function of the inclination of the constellation i, the angle δ describing the separation of the satellites, the capability of the on-board propulsion described by $\alpha_{\max}$, and the rule defining how far satellites are allowed to drift apart in RAAN by $\Delta\Omega_{\max}$ before their orbits are corrected by propulsive impulse $\Delta V_{\rm cor}$. First, the optimal corrective impulse is determined by (14) and the differential regression of nodes determined by the derivative of (1a)

$$\Delta\dot{\Omega} = \frac{3}{2} n J_2 \left(\frac{R_{\rm eq}}{p}\right)^2 \sin i \, \delta. \tag{15}$$

The lifetime of the mission is governed by the satellite with $\Delta i = \delta$, the satellite which requires the greatest rate of propulsion expenditure and, hence, would be the first to consume all of its propulsion and drift out of the constellation. Second, the ideal rate of propulsion expenditure is determined according to (8) and the effective rate of propulsion expenditure by (12).

As a general rule of thumb, optimal propulsion efficiency is achieved with a strict limitation on the amount of drift in RAAN $\Delta\Omega_{\max}$ before propulsive maneuvering is necessary to bring a satellite back in to the formation

$$|\Delta\Omega_{\max} \sin i| \ll \frac{2\alpha_{\max}}{n^2 a}. \tag{16}$$

This follows from $\eta \to 1$ and, hence, $\gamma \to 0$. Finally, the lifetime of the constellation is limited by the separation of the satellites δ

$$\tilde{\alpha}^{-1} \simeq \left[\frac{3}{2} n^2 a \sin^2 i \, J_2 \left(\frac{R_{\rm eq}}{p}\right)^2 \delta\right]^{-1} \tag{17}$$

and the mission lifetime $L = \tilde{\alpha}^{-1} \Delta V_{\rm total}$ where $\Delta V_{\rm total}$ is the amount of on-board propulsion *after* the satellites' orbits are configured.

While the particular application is to a constellation of RO satellites for the tomography of internal gravity waves, many of the same rules apply for maintaining a constellation of satellites that fly in a close formation but experience differential rates of regression of nodes. In the general case, (16) and (17) apply for the efficiency of propulsion expenditure and the approximate lifetime of the mission.

Simulations using a realistic, comprehensive orbit propagator show that cold gas propulsion systems enable constellations with greater intersatellite separations δ than electrospray propulsion systems but deliver much shorter mission lifetimes than eletrospray propulsion systems do. The much greater accelerations $\alpha_{\max}$ provided by cold gas systems allow for greater differential rates of regression of nodes $\Delta\dot{\Omega}$ and, hence, also greater separations δ between satellites in the constellation. The greater *total* propulsion ΔV offered by electrospray systems—because of the much greater specific impulse they offer—leads to much longer mission lifetimes than cold gas propulsion systems can

provide. In fact, cold gas systems lead to mission lifetimes of less than ∼100 days while electrospray systems can deliver mission lifetimes in excess of ∼1000 days.

Relative station keeping will also require maneuvering to counter the effects of differential atmospheric drag and smaller gravitational perturbations, but the differential forces involved are far less than the forces involved in the differential regression of nodes. For a 6 U CubeSat, the neutral atmospheric drag near the ISS orbit is estimated to range from 0.1 to 1.0 m s^{-1} day^{-1}, and the *differential* neutral atmospheric drag between the satellites in the constellation much less than that. All rates of propulsion expenditure necessary to counter the differential regression of nodes exceed 2 m s^{-1} day^{-1}; thus, considering the countering of the differential regression of nodes as the primary demand on propulsion is justified. Nevertheless, a future mission demonstration simulation should include a more realistic scenario of orbital perturbations and maneuvers needed to counteract them.

The long mission lifetimes that electrospray propulsion systems can deliver almost certainly dictates that CubeSat formation flying requires electrospray propulsion. In the case of RO, two significant challenges remain, namely that the amount of separation between satellites in a constellation is extremely limited (to $\sim 0.1^\circ$) and that the fraction f of time spent in propulsive maneuvering can be large. Internal gravity wave tomography will require spacecraft separations of ∼100 km, corresponding to spacecraft separations of $\sim 1^\circ$, which is not currently attainable with electrospray propulsions. The fraction of time spent in propulsive maneuvering can be estimated as

$$f = \frac{\Delta V_{\text{cor}}}{\alpha_{\max}} \frac{|\Delta \dot{\Omega}|}{\Delta \Omega_{\max}} \tag{18}$$

see (14). When the separations δ approach their limiting value, the fraction f approach 100%. RO requires that the orbital velocity be known to $0.4\ \text{mm s}^{-1}$, and presently no orbit determination system is capable of such precision during propulsive maneuvering. To address both challenges, we recommend that electrospray propulsion systems develop a greater capacity for thrust. We expect that the instantaneous electrical power demand will increase in proportion to the amount of thrust electrospray propulsion can generate; however, the fraction of time spent in propulsive maneuvering will decrease in approximately inverse proportion to the thrust, thus conserving the orbit-average power consumed by propulsion. Careful scheduling and management of power on board CubeSats would have to be emphasized.

Appendix A
Constructing a Mutually Orbiting Group

A mutual orbiting group of satellites is defined with respect to a reference circular orbiter $j = 0$. The specific angular momentum of the reference orbiter is $\mathbf{l}_0$

$$\mathbf{l}_0 = \bar{n} a^2 \hat{\mathbf{l}}_0 \tag{19}$$

in which $\bar{n}$ is the mean motion of the orbit, and the angular momentum for a satellites in the group is

$$\mathbf{l} = \bar{n} a^2 \sqrt{1 - e^2}\, \hat{\mathbf{l}}. \tag{20}$$

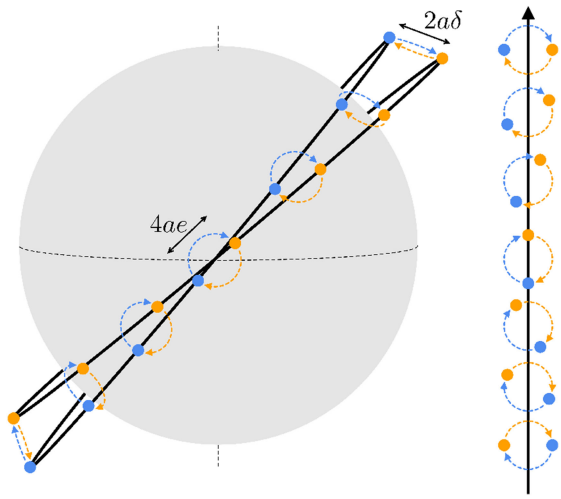

Fig. 7. Mutual orbiting pair. The reference circular orbit would be in the center of all the circles on the right, each circle mapping out the mutual orbit trajectory. Clockwise motion requires $s = +1$.

Equation (4b) describes how the semimajor axis must be perturbed to account for rates of regression of nodes and precession of perigee, but for the sake of constellation design, the semimajor axis a is assumed to be the same for all satellites. The mutually orbiting group of satellites is designed to move in an elliptical trajectory around the reference circular orbiter, the trajectory having axis length $4ae$ parallel to the velocity vector and axis length $2a\delta$ in the transverse direction; e is the semimajor axis and eccentricity of the mutual orbiter and δ is defined below. Fig. 7 illustrates a mutual orbiting group of two satellites.

The following coordinate system is used to construct the mutually orbiting group: $\hat{\mathbf{x}}$ points in the direction of the ascending node of the reference orbiter, $\hat{\mathbf{z}}$ along the Earth's spin axis, and $\hat{\mathbf{y}}$ in the equatorial plane such that $\hat{\mathbf{x}} \times \hat{\mathbf{y}} = \hat{\mathbf{z}}$. The direction of angular momentum of the reference orbit is

$$\hat{\mathbf{l}}_0 = \cos i_0\, \hat{\mathbf{z}} - \sin i_0\, \hat{\mathbf{y}} \tag{21}$$

in which i_0 is the inclination of the reference orbiter. A coordinate system associated with the orbit of the reference orbiter is defined as $(\hat{\mathbf{x}}, \hat{\mathbf{l}}_0, \hat{\mathbf{m}}_0)$ such that $\hat{\mathbf{m}}_0 = \hat{\mathbf{l}}_0 \times \hat{\mathbf{x}}$. The direction of angular momentum of a mutual orbiting satellite is just a small departure from that of the reference orbiter

$$\hat{\mathbf{l}} = \cos\delta\, \hat{\mathbf{l}}_0 + \sin\delta \cos\theta\, \hat{\mathbf{m}}_0 + \sin\delta\ \sin\theta\, \hat{\mathbf{x}}. \tag{22}$$

The angles δ and θ are the separation of the angular momentum vectors of the reference orbiter and that of the mutually orbiting satellite and an angle describing the position of the mutual orbiter with respect to the reference orbiter when the reference orbiter is at its ascending node. See Fig. 8 for a diagram of the basis vectors describing the coordinate systems. The inclination i of the mutual orbiting satellite is determined by

$$i = \arccos(\hat{\mathbf{l}} \cdot \hat{\mathbf{z}}) \tag{23}$$

and the RAAN Ω of the mutual orbiter is

$$\Omega = \Omega_0 + \arctan(\hat{\mathbf{l}} \cdot \hat{\mathbf{x}}, -\hat{\mathbf{l}} \cdot \hat{\mathbf{y}}). \tag{24}$$

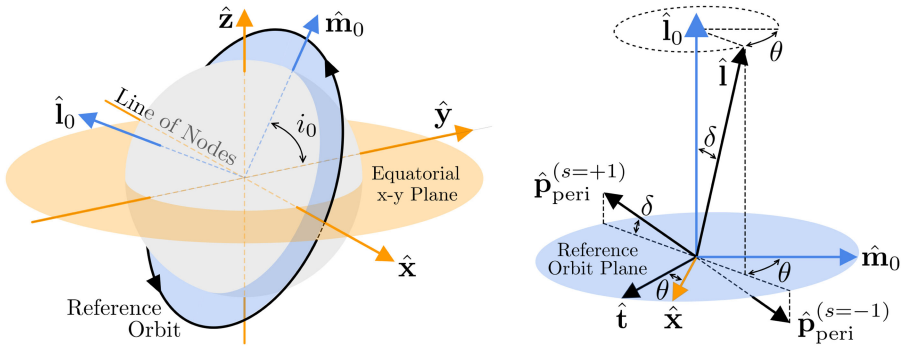

Fig. 8. Coordinate system and directional vectors used in computing the orbital elements of the satellites in a mutually orbiting group. The unit vectors $\hat{\mathbf{l}}_0, \hat{\mathbf{l}}$ point in the direction of the angular momenta of the reference orbiter and of a satellite in the mutually orbiting group; $\hat{\mathbf{x}}$ toward the ascending node of the satellite being configured assuming $\Omega_0 = 0$; and $\hat{\mathbf{z}}$ the Earth's spin angular momentum. Perigee is shown for a clock mutual orbit ($s = +1$) and a counter-clockwise mutual orbit ($s = -1$). The plot on the left shows some of the vectors using the Earth's equatorial plane for perspective; the plot on the right using the reference orbit plane for perspective. All vectors, angles, and scalars are described in Appendix A.

The four-quadrant arctangent takes two arguments and is described by $\gamma = \arctan(q \sin\gamma, q\cos\gamma)$, the scalar q being any positive scalar. The quantity Ω_0 is the RAAN for the reference orbiter. The direction of the ascending node of the mutual orbiter with respect to the Earth's center of mass is

$$\hat{\mathbf{p}}_{\text{node}} = \cos(\Omega - \Omega_0)\,\hat{\mathbf{x}} + \sin(\Omega - \Omega_0)\,\hat{\mathbf{y}}. \tag{25}$$

In order to determine the remaining elements of the mutual orbiter, it is convenient to describe the "direction of intersection" of the mutual orbiter and the reference orbiter. The direction of intersection is

$$\hat{\mathbf{t}} = \csc\delta\,\hat{\mathbf{l}} \times \hat{\mathbf{l}}_0. \tag{26}$$

It is possible to define the direction of perigee of the mutual orbiter by simple argument. When the circular orbiter is at the direction of intersection, the mutual orbiter must be either directly in front of or directly behind the reference orbiter, using the velocity vector of the reference orbiter as the direction "forward." When in one of those positions, the eccentric orbiter must be moving with the same speed as the circular orbiter. This means that the mutual orbiter must be at its perigee when the circular orbiter is $\pi/2$ radians away from the direction of intersection $\hat{\mathbf{t}}$. Thus, the perigee direction is

$$\hat{\mathbf{p}}_{\text{peri}} = s\,\hat{\mathbf{t}} \times \hat{\mathbf{l}} \tag{27}$$

with s indicating whether the orbiter travels clockwise ($s = +1$) or counter-clockwise ($s = -1$) around the reference orbiter. The argument of perigee ω can be determined with the help of an auxiliary direction $\hat{\mathbf{m}} = \hat{\mathbf{l}} \times \hat{\mathbf{p}}_{\text{node}}$

$$\omega = \arctan(\ \hat{\mathbf{p}}_{\text{peri}} \cdot \hat{\mathbf{m}},\ \hat{\mathbf{p}}_{\text{peri}} \cdot \hat{\mathbf{p}}_{\text{node}}\ ). \tag{28}$$

The only remaining Keplerian orbital element required to describe the orbit of the mutual orbiter is the true anomaly ν at a specific epoch. From the time the reference orbiter is at its ascending node ($\hat{\mathbf{x}}$) to the time it is at intersection $\hat{\mathbf{t}}$ multiplied by the mean motion $\bar{n}$ is

$$\bar{n}(t_{\text{intersection}} - t_{\text{node},0}) = \arctan(\ \hat{\mathbf{t}} \cdot \hat{\mathbf{m}}_0,\ \hat{\mathbf{t}} \cdot \hat{\mathbf{x}}\ ). \tag{29}$$

The time from intersection for the circular orbiter to the time of perigee for the mutual orbiter multiplied by the mean motion is

$$\bar{n}(t_{\text{perigee}} - t_{\text{intersection}}) = -s\pi/2. \tag{30}$$

Putting the last two equations together gives the amount of time from the mutual orbiter passing through its perigee to the time when the circular orbiter passes through its ascending node

$$\bar{n}(t_{\text{node},0} - t_{\text{perigee}}) = \arctan(\ s\hat{\mathbf{t}} \cdot \hat{\mathbf{x}}, s\hat{\mathbf{t}} \cdot \hat{\mathbf{m}}_0\ ). \tag{31}$$

The eccentric anomaly ψ of the mutual orbiter when the reference orbiter is at its ascending node is given by

$$\psi - e\sin\psi = \bar{n}(t_{\text{node},0} - t_{\text{perigee}}) \tag{32}$$

which requires iteration to find ψ [21]. Once the eccentric anomaly is known, the true anomaly ν of the mutual orbiter can be determined from the eccentric anomaly ψ. The relationship between the two is given by

$$\nu = \arctan(\sin\psi\sqrt{1-e^2}, \cos\psi - e) \tag{33a}$$

$$\psi = \arctan(\sin\nu\sqrt{1-e^2}, \cos\nu + e). \tag{33b}$$

This relationship is perfect for ideal Keplerian orbits but imperfect for orbits subjected to the noncentral J_2 gravitational anomaly. The latter case is pertinent to this article, and the departures in the eccentric and true anomalies are on the order of J_2 in radians.

ACKNOWLEDGMENT

The authors would like to acknowledge Analytical Graphics, Inc., for use of the Systems Tool Kit (STK) and the U.S. National Aeronautics and Space Administration for use of the General Mission Analysis Tool (GMAT). STK was used under a purchased license and GMAT under an open license.

REFERENCES

[1] J. Holton, *An Introduction to Dynamic Meteorology*, 3rd ed. New York, NY, USA: Academic, 1992.
[2] D. Fritts and M. Alexander, "Gravity wave dynamics and effects in the middle atmosphere," *Rev. Geophys.*, vol. 41, no. 1, pp. 1–68, 2003.

[3] M. Alexander *et al.*, "Review article: Recent developments in gravity-wave effects in climate models and the global distribution of gravity-wave momentum flux from observations and models," *Quart. J. Roy. Meteorol. Soc.*, vol. 136, pp. 1103–1124, 2010.

[4] R. Lindzen and J. Holton, "A theory of the quasi-biennial oscillation," *J. Atmos. Sci.*, vol. 25, no. 6, pp. 1095–1107, 1968.

[5] J. Holton, P. Haynes, M. McIntyre, A. Douglass, R. Rood, and L. Pfister, "Stratosphere-troposphere exchange," *Rev. Geophys.*, vol. 33, no. 4, pp. 403–439, 1995.

[6] M. P. Baldwin *et al.*, "The quasi-biennial oscillation," *Rev. Geophys.*, vol. 39, no. 2, pp. 179–229, 2001.

[7] G. Mastrantonio, F. Einaudi, D. Fua, and D. Lalas, "Generation of gravity waves by jet streams in the atmosphere," *J. Atmos. Sci.*, vol. 33, pp. 1730–1738, 1977.

[8] C. Homeyer, J. McAuliffe, and K. Bedka, "On the development of above-anvil cirrus plumes in extratropical convection," *J. Atmos. Sci.*, vol. 74, pp. 1617–1633, 2017.

[9] R. Smith, "Travelling waves and bores in the lower atmosphere: the 'morning glory' and related phenomena," *Earth-Sci. Rev.*, vol. 25, no. 4, pp. 267–290, 1988.

[10] E. Dewan and R. Picard, "Mesospheric bores," *J. Geophys. Res.*, vol. 103, no. D6, pp. 6295–6305, 1998.

[11] B. Karlsson and T. Shepherd, "The improbable clouds at the edge of the atmosphere," *Phys. Today*, vol. 71, no. 6, pp. 30–36, 2018.

[12] E. Kursinski, G. Hajj, J. Schofield, R. Linfield, and K. Hardy, "Observing Earth's atmosphere with radio occultation measurements using the global positioning system," *J. Geophys. Res.*, vol. 102, no. D19, pp. 23429–23465, 1997.

[13] G. Hajj, E. Kursinski, L. Romans, W. Bertiger, and S. Leroy, "A technical description of atmospheric sounding by GPS occultation," *J. Atmos. Solar-Terrestrial Phys.*, vol. 64, no. 4, pp. 451–469, 2002.

[14] T. Tsuda, M. Nishida, C. Rocken, and R. Ware, "A global morphology of gravity wave activity in the stratosphere revealed by the GPS occultation data (GPS/MET)," *J. Geophys. Res.*, vol. 105, no. D6, pp. 7257–7273, 2000.

[15] C. Marquardt and S. Healy, "Measurement noise and stratospheric gravity wave characteristics obtained from GPS occultation data," *J. Meteorol. Soc. Japan*, vol. 83, pp. 417–428, 2005.

[16] D. Wu *et al.*, "Remote sounding of atmospheric gravity waves with satellite limb and nadir techniques," *Adv. Space Res.*, vol. 37, pp. 2269–2277, 2006.

[17] L. Hoffmann and M. Alexander, "Retrieval of stratospheric temperatures from Atmospheric Infrared Sounder radiance measurements for gravity waves studies," *J. Geophys. Res.*, vol. 114, 2009, doi:10.1029/2008JD011241.

[18] L. Wang and M. Alexander, "Global estimates of gravity wave parameters from GPS radio occultation temperature data," *J. Geophys. Res.*, vol. 115, 2010, doi:10.1029/2010JD013860.

[19] T. Schmidt, P. Alexander, and A. de la Torre, "Stratospheric gravity wave momentum flux from radio occultations," *J. Geophys. Res.*, vol. 121, pp. 4443–4467, 2016.

[20] J. Tollefson, "Weather-data race heats up," *Nature*, vol. 542, 2017, Art. no. 18.

[21] H. Goldstein, *Classical Mechanics*, 2nd ed. Reading, MA, USA: Addison Wesley, 1980.

Stephen Leroy received the B.A. degree in physics from Cornell University, Ithaca, NY, USA, in 1988, and the M.Sc. and Ph.D. degrees in planetary science from the California Institute of Technology, Pasadena, CA, USA in 1990 and 1994, respectively.

He is currently a Principal Scientist with Atmospheric and Environmental Research, Inc., Lexington, MA, USA. His previous positions were as a Scientist with the NASA Jet Propulsion Laboratory (1994–2004) and as a Project Scientist in Prof. J. Anderson's Group at Harvard University (2004–2017). His research interests include covered atmospheric internal gravity waves, GNSS radio occultation, nadir spectral infrared sounding, detection and attribution of climate change, and Bayesian information theory applied to remote sensing data types.

Riley Fitzgerald received the B.S.E. degree in mechanical and aerospace engineering from Princeton University, Princeton, NJ, USA, in 2016, and the M.S. degree in aeronautics and astronautics in 2018 from the Massachusetts Institute of Technology (MIT), Cambridge, MA, USA, where he is currently working toward the Ph.D. degree with the Department of Aeronautics and Astronautics.

He works with the Space Telecommunications, Astronomy, and Radiation Laboratory, MIT, as a Draper Fellow. His research interests primarily include orbital mechanics and spacecraft navigation.

Kerri Cahoy (Member, IEEE) received the B.S. degree in electrical engineering from Cornell University, Ithaca, NY, USA, in 2000, and the M.S. and Ph.D. degrees in electrical engineering from Stanford University, Stanford, CA, USA, in 2002 and 2008, respectively.

She is an Associate Professor of aeronautics and astronautics with the Massachusetts Institute of Technology, Cambridge, MA, USA, and leads the Space Telecommunications, Astronomy, and Radiation Laboratory. She previously was with Space Systems Loral, as a Postdoctoral Fellow with NASA AMES, and currently leads nanosatellite atmospheric sensing, optical communications, and exoplanet technology demonstration missions.

James Abel is an undergraduate Research Assistant who is studying aerospace engineering with the Massachusetts Institute of Technology, Cambridge, MA, USA. He built the models used to track the motion of the satellites, and analyzed the resulting data. In addition to research, he is currently contributing to a number of other projects, including developing an electric aircraft and building a rocket to get to space.

James Clark received the S.B. and S.M. degrees in aeronautics and astronautics in 2014 and 2016, respectively, from the Massachusetts Institute of Technology, Cambridge, MA, USA, where he is currently working toward the Ph.D. degree with the Department of Aeronautics and Astronautics.

His research interests primarily include laser communication, mission and trajectory design, and advanced concept development.